Journal of Materials Chemistry A

Lead-Free Low-Dimensional Tin Halide Perovskites with Functional Organic Spacers: Breaking the Charge-Transport Bottleneck

Journal:	*Journal of Materials Chemistry A*
Manuscript ID	TA-COM-04-2019-004486.R1
Article Type:	Paper
Date Submitted by the Author:	18-Jun-2019
Complete List of Authors:	Ju, Ming-Gang; University of Nebraska-Lincoln Dai, Jun; University of Nebraska-Lincoln, Chemistry Ma, Liang; Southeast University, School of Physics Zhou, Yuanyuan; Brown University, School of Engineering Liang, WanZhen; Xiamen university, Zeng, Xiao Cheng; University of Nebraska-Lincoln, Department of Chemistry

Journal Name

ARTICLE

Lead-Free Low-Dimensional Tin Halide Perovskites with Functional Organic Spacers: Breaking the Charge-Transport Bottleneck

Received 00th Month 20xx,
Accepted 00th Month 20xx

DOI: 10.1039/x0xx00000x

www.rsc.org/

Minggang Ju,[a] Jun Dai,[a] Liang Ma,[b] Yuanyuan Zhou,[c] Wanzhen Liang[d] and Xiao Cheng Zeng[ae*]

Low-dimensional organic-inorganic halide perovskites (OIHPs) have received intense interest due largely to their remarkable stability compared to the 3D counterparts for potential optoelectronic and photovoltaic (PV) applications,. However, 2D OIHPs encounter a 'bottleneck' of ultra-low conductivity between the inorganic sheets, owing to the intrinsic quantum and dielectric confinement, which usually results in unsatisfactory device performance. Herein, we predict and design a new family of 2D OIHPs to break the charge-transport 'bottleneck'. The newly designed 2D OIHPs consist of π-conjugation organic species as the spacers. As such, we find that the electronic structures exhibit type-II band alignment (staggered bandgap). Such a band-structure feature by design, if confirmed in the laboratory, reenforces a materials-design strategy for enhancing optoelectronic or PV device performance with the 2D OIHPs.

Introduction

The state-of-the-art polycrystalline thin-film perovskite solar cells (PSCs) have achieved power conversion efficiency (PCE) of 23.7%.[1] This is the fastest rise in PCE among any class of photovoltaic absorber materials.[2] The highly cost-effective PSCs with the high PCE have strong implications that the next-generation high performance semiconductors are halide perovskites.[3-11] However, the large-scale application of OIHP-based PSCs are still hampered by the instability and toxicity issues due to their containing of hygroscopic organic (e.g., methylammonium (MA^+) or formanidium (FA^+)) and lead (Pb) cations.[12] To address both issues, extensive research effort has been devoted to seeking highly stable and lead-free perovskites for PVs.[13-21] Recently, low-dimensional OIHPs have received intense attention owing to their robust ambient stability.[22-31] Among the low-dimensional OIHPs, 2D Ruddleson-Popper (RP) perovskites have been extensively studied since relatively high PV performance can be achieved by controlling the crystallographic anisotropy in the thin films.[32] Indeed, the associated devices have yielded the PCE of 14%.[33, 34] However, the 2D RP OIHP is still based on the toxic element, lead, while the PCE is still notably lower than that of 3D OIHPs. Another known type of 2D OIHP, namely, Dion-Jacobson (DJ) phase, has also been synthesized[35] recently, and the associated devices based on DJ tin halide perovskites have yielded a PCE of 4.22%.[36]

Note that 2D OIHPs are essentially quantum-well structures formed by *n* blocks of inorganic $[PbI_6]^{4-}$ octahedral slab, each slab being separated by bulky organic cations such as monoammonium cation in the RP phase, and diammonium cation in the DJ phase. Most 2D OIHPs exhibit the type-I electronic band alignment of the organic and inorganic frameworks.[37-40] Because of their quantum-well structures, 2D OIHPs typically exhibit strong effects of quantum confinement and dielectric confinement. As a result, the charges are generally confined to the inorganic framework, and the exciton binding energies can be many times greater than kT at room temperature (k is the Boltzmann constant and T is temperature). Both physical features are undesirable for PV devices.[41] Moreover, the optical bandgaps of 2D OIHPs are wider than those of 3D counterparts. It is known that both strong light absorption in visible range and the easy separation of electron-hole pairs are important requests for high performance PV devices. In most 2D OHIPs, excitons tend to recombine rather than dissociate into free electrons and holes. Nevertheless, we propose that 2D OIHPs with type-II band alignment can significantly facilitate the separation of excitons to overcome the limitations of prevailing 2D OIHPs with type-I band alignment. To our knowledge, only a few of type-II compounds have been reported.[42, 43]

In general, the "organic" component in 2D OIHPs possesses smaller dielectric constant than the inorganic component, resulting in type-I band alignment. To design 2D OHIPs with the type-II band alignment, "organic" component with higher dielectric constant is required. Recently, Liu et al. have proposed to tune the optoelectronic properties by changing specific organic functional groups.[44] It is known that organic semiconductors composed of π-conjugation molecules possess higher dielectric constants, which can lead to higher carrier mobility. Most of these π-conjugation molecules are commercially available at low-cost, such as oligoacenes and

[a] Department of Chemistry, University of Nebraska–Lincoln
[b] Southeast University, Nanjing 211189, China
[c] School of Engineering, Brown University, Providence, Rhode Island 02912, United States
[d] State Key Laboratory of Physical Chemistry of Solid Surfaces, Collaborative Innovation Center of Chemistry for Energy Materials, Fujian Provincial Key Laboratory of Theoretical and Computational Chemistry, and Department of Chemistry, College of Chemistry and Chemical Engineering, Xiamen University, Xiamen, Fujian 361005, China
[e] Department of Chemical & Biomolecular Engineering and Department of Mechanical & Materials Engineering, University of Nebraska-Lincoln, Lincoln, Nebraska, 68588, United States

oligothiophenes.[45, 46] With these prototypical π-conjugation molecules, the corresponding cations can be obtained by chemical modification. Herein, we report a series of 2D lead-free OIHPs, (π-DAM)$(FA)_{n-1}Sn_nX_{3n+1}$ (n = 1 - 4), where π-DAM refers to an organic diammonium cation with π-conjugation molecular structure [i.e., 2,6-anthracenediyldimethanammonium (AMA), 2,8-tetracenediyldimethanammonium (TMA), 2,9-pentacenediyldimethanammonium (PMA), 2,10-hexacenediyldimethanammonium (HMA), or anthra[2,3-b:7,8-b']bis(5-thiopheneylmethanammonium) (ATMA)]. Here, X refers to halogen anion (i.e., I, Br or Cl). Based on the DFT computation, we systematically investigate these 2D compounds. By introducing different π-DAM, we can effectively alter the optoelectronic properties of 2D OIHPs to possess the type-II band alignment, thereby facilitating separation of electron-hole pairs to enhance carrier mobility.

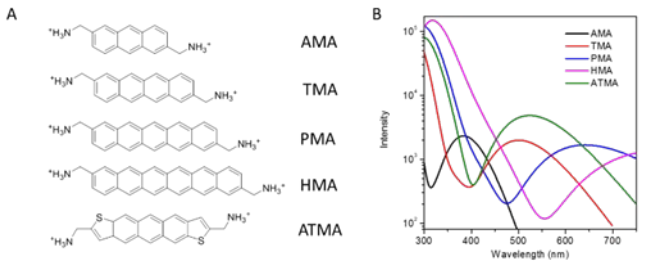

Figure 1. (A) Molecular structures of selected π-DAMs considered in the study. (B) Computed optical absorption spectra of π-DAMs by using TD-DFT method.

Results and discussion

In this study, we focus on the 2D DJ OIHPs. Fig. 1A shows the five organic molecular structures of π-DAMs considered. All the π-DAMs are derivatives of oligoacenes which have been widely studied molecular semiconductors. For oligoacenes, particular attention is placed on the pentacene and tetracene due to their high carrier mobility. The main building blocks of oligoacenes (anthracene, tetracene, pentacene and hexacene) are benzene rings (ranging from 3 to 6), all connected in a planar fashion except anthra[2,3-b:7,8-b']dithiophene which may be viewed as a variant of pentacene. For the latter, two benzenes located at both ends of pentacene are substituted by thiophenes. Electronic Supplemental Information (ESI) Fig. S1 shows the highest occupied molecular orbital (HOMO) and the lowest unoccupied molecular orbital (LUMO) of the five π-DAMs considered. The energy level of HOMO rapidly increases with increasing of the number of benzene rings, while that of LUMO slowly increases, resulting in gradually narrowed bandgap with increasing of the number of benzene rings. Moreover, the energy level of the ATMA HOMO is located between that of PMA and HMA, while the energy level of the ATMA LUMO is between that of TMA and PMA, suggesting two strategies to alter the electronic properties of π-DAMs: (1) Changing the number of benzene rings, and (2) substituting benzene with another aromatic cycle, like thiophene. The different frontier energy levels of π-DAMs imply that the band alignment of 2D OIHPs may be altered by introducing different π-DAMs. Fig. 1B displays the computed optical absorption spectra with different π-DAMs. Clearly, all π-DAMs yield suitable optical absorption in the visible range, desired for PV application.

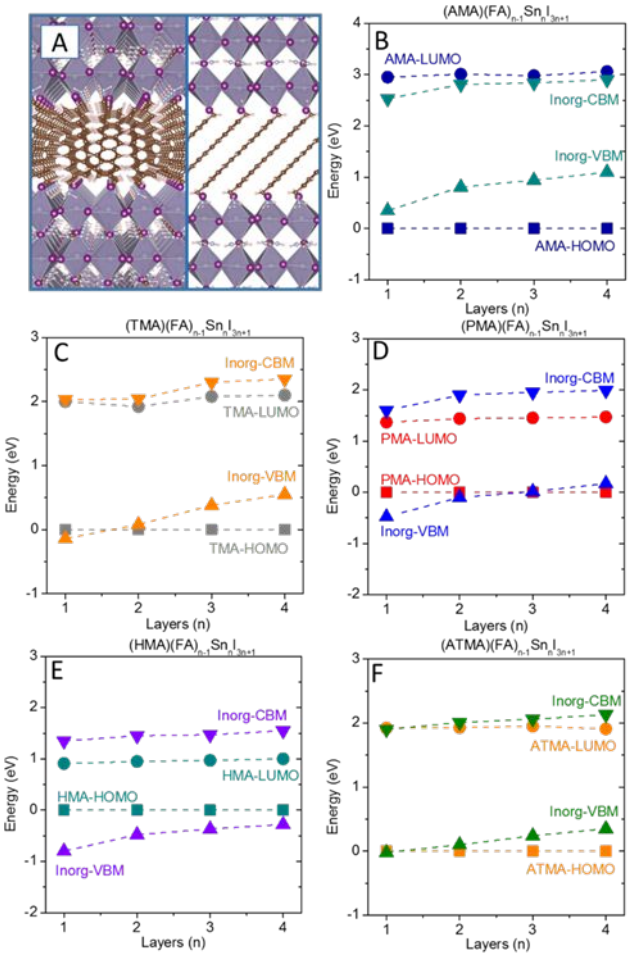

Figure 2. Crystalline structures of 2D OIHPs (π-DAMs$(FA)_{n-1}Sn_nX_{3n+1}$ viewed from front (left panels) and side (right panels) (A). Computed frontier energy level of "organic" and "inorganic" components of (π-DAM)$(FA)_{n-1}Sn_nI_{3n+1}$ (n = 1 - 4), π-DAM = AMA (B), TMA (C), PMA (D), HMA (E) and ATMA (F), based on the PBE0 functional. The computed HOMO of "organic" components is treated as the reference energy.

For 2D OIHPs, four different band alignments (type-Ia, type-Ib, type-IIa, and type-IIb) are possible (see Fig. S2). Type-I band alignment is not beneficial to PV application. Fig. 2A shows the crystal structures of 2D DJ OIHPs. It can be seen that π-DAMs with tilt angle are embedded between inorganic scaffold (more structural details are given in Fig. S3). Firstly, we consider the compounds with formula (π-DAM)$(FA)_{n-1}Sn_nI_{3n+1}$ (n = 1 - 4). With different π-DAMs, the electronic properties of these compounds are computed, including their frontier energy levels and bandgaps, based on the PBE0 functional. The frontier energy levels of "organic" and "inorganic" components with different inorganic layers (n = 1 - 4) are displayed in Fig. 2B-2F. Clearly, compounds with formula (AMA)$(FA)_{n-1}Sn_nI_{3n+1}$ (n = 1 - 4) possess type-Ib band alignment of organic and inorganic frameworks due to high LUMO energy level and low

HOMO energy level of AMA. Interestingly, when TMA is introduced into the 2D OIHPs, the band alignment of the compounds with formula $(TMA)(FA)_{n-1}Sn_nI_{3n+1}$ (n = 1 - 4) is converted from the type-Ia to type-IIa, with increasing of the number of "inorganic" layers (see Fig. 2C). For compounds with $(PMA)(FA)_{n-1}Sn_nI_{3n+1}$ (n = 1 - 4), again, the band alignment is converted from the type-Ia to type-IIa. The difference between $(TMA)(FA)_{n-1}Sn_nI_{3n+1}$ and $(PMA)(FA)_{n-1}Sn_nI_{3n+1}$ is that at n = 2, the band alignment is already changed to the type-IIb for the former, whereas for the latter at n = 3, the band alignment is changed to the type-IIa. All compounds with formula $(HMA)(FA)_{n-1}Sn_nI_{3n+1}$ (n = 1 - 4) possess the type-Ia band alignment due to the low LUMO energy level and high HOMO energy level of HMA.

As aforementioned, ATMA possesses similar electronic properties as TMA and PMA. For compounds with formula $(ATMA)(FA)_{n-1}Sn_nI_{3n+1}$ (n = 1 - 4), at n = 2, the band alignment also is changed to the type-IIa with increasing of the number of layers. Interestingly, the band alignment of compound $(ATMA)SnI_4$ belongs to the type-IIb. Based on our analysis, four band alignments are possible in the newly designed compounds. These account for different band alignments for 2D OIHPs through altering the organic cation and the number of layers of inorganic scaffold. In addition, for all the compounds, the frontier energy levels of "inorganic" components gradually increase with increasing of the number of layers with respect to the corresponding "organic" components. Meanwhile, the bandgap of "organic" component is hardly changed with increasing of the number of layers, indicating that the thickness of inorganic scaffold has little effect on the organic cations. In contrast, the bandgap of "inorganic" component gradually decreases with increasing of the number of layers.

Next, if iodine in the compounds is substituted by another halogen element (e.g., Br and Cl), the electronic properties of inorganic scaffold would be significantly modified. Fig. S4A-E and Fig. S5A-E show the frontier energy levels of $(\pi\text{-DAM})(FA)_{n-1}Sn_nBr_{3n+1}$ (n = 1 - 4) and $(\pi\text{-DAM})(FA)_{n-1}Sn_nCl_{3n+1}$ (n = 1 - 4), respectively. It can be seen that bromide and chloride result in wider bandgap for "inorganic" component. Due to the relatively high energy level of CBM and relatively low energy level of VBM, most compounds possess the type-Ia band alignment except $(AMA)(FA)_{n-1}Sn_nBr_{3n+1}$ (n = 2 - 4) and $(AMA)(FA)_{n-1}Sn_nCl_{3n+1}$ (n = 3 - 4), which possess the type-IIa band alignment. In addition, the electronic properties of "inorganic bromide" component and "inorganic chloride" component exhibit similar trend as iodide. For example, the frontier energy levels of "inorganic" component gradually increase with the increasing of the number of layers with respect to the corresponding "organic" components. Due to the stronger interaction between "organic" and "inorganic" components, the bandgap of "organic" component associated with bromide and chloride is narrower than that associated with iodide, a manifestation of stronger electronegativity of bromine and chloride ion.

Compounds with formula $(TMA)(FA)_{n-1}Sn_nI_{3n+1}$ (n = 2 - 4), $(PMA)(FA)_{n-1}Sn_nI_{3n+1}$ (n = 3 - 4), $(ATMA)(FA)_{n-1}Sn_nI_{3n+1}$ (n = 1 - 4), $(AMA)(FA)_{n-1}Sn_nBr_{3n+1}$ (n = 2 - 4), and $(AMA)(FA)_{n-1}Sn_nCl_{3n+1}$ (n = 3 - 4) all possess the type-II band alignment, which is potentially beneficial to PV application. Figs. S6-S10 show the total density of states (TDOS) and projected density of states (PDOS) of these compounds. The HOMO and LUMO of "organic" component are mainly contributed by the π-conjugation of π-DAMs. The CBM of "inorganic" component is mostly contributed by Sn *p* orbital while the VBM of "inorganic" component is mostly contributed by halogen *s* orbital and Sn *p* orbital, similar to the 3D tin halide perovskites. As pointed out above, the energy levels of VBM and CBM of "inorganic" component shift significantly, with respect to HOMO and LUMO of "organic" component, with increasing of the number of layers. Fig. S11 shows the charge density distribution corresponding to CB and VB around the band edge for compounds $(PMA)(FA)_{n-1}Sn_nI_{3n+1}$ (n = 1 - 4). Clearly, for n = 1 and 2, VBM and CBM that exhibit π-conjugation orbitals are localized on PMA, confirming that $(PMA)(FA)_{n-1}Sn_nI_{3n+1}$ (n = 1, 2) possess the type-Ia band alignment. For n = 3, the VBM is delocalized on both "inorganic" and "organic" components, and the CBM is localized on the "organic" component, demonstrating that there is a transition of band alignment from the type-Ia to type-IIa. For n = 4, $(PMA)(FA)_3Sn_4I_{13}$ possesses the type-IIa band alignment, while the VBM with characters of Sn *s* orbital and I *p* orbital is localized on the "inorganic" component, and the CBM with characters of π-conjugation orbitals is localized on the "organic" component.

As pointed out above, compounds possessing the type-II band alignment are expected to facilitate the separation of hole-electron pairs (see Fig. 3A), which may improve performance of PV device. Considering 2D OIHPs as a light absorber, the increasing of number of layers of "inorganic" component seems beneficial to light absorption in visible region. For n = 4, there is stronger light absorption in the visible range for compounds $(TMA)(FA)_{n-1}Sn_nI_{3n+1}$, $(PMA)(FA)_{n-1}Sn_nI_{3n+1}$ and $(ATMA)(FA)_{n-1}Sn_nI_{3n+1}$. Meanwhile, $(AMA)(FA)_3Sn_4Br_{13}$ and $(ATMA)(FA)_3Sn_4Cl_{13}$ possess wider bandgap (>2.5 eV and 3.0 eV, respectively), unsuitable for the light absorption in the visible region. Hereafter, we mainly focus on the three newly designed compounds, $(TMA)(FA)_3Sn_4I_{13}$, $(PMA)(FA)_3Sn_4I_{13}$ and $(ATMA)(FA)_3Sn_4I_{13}$. To gain deeper insight into the effect of π-DAMs on band alignment, we compute band structures of $(TMA)(FA)_3Sn_4I_{13}$, $(PMA)(FA)_3Sn_4I_{13}$ and $(ATMA)(FA)_3Sn_4I_{13}$ compound, respectively. Fig. 3C-3D shows the band structures of $(TMA)(FA)_3Sn_4I_{13}$, $(PMA)(FA)_3Sn_4I_{13}$ and $(ATMA)(FA)_3Sn_4I_{13}$. The states of π-DAMs are identified with orange color in the projected density of states (PDOS). The *K* path in the reciprocal space is shown in Fig. 3B. One can see that all three compounds exhibit similar contour features of the band structures, and all exhibits a direct bandgap at the Z point due to similar properties of the three diammoniums (TMA, PMA and ATMA). By changing the π-DAM, the dispersive bands due to the "organic" component shift with respect to those due to the "inorganic" component, consistent with the feature illustrated in PDOS. In contrast, the "inorganic" component derived band exhibits little change for the three compounds.

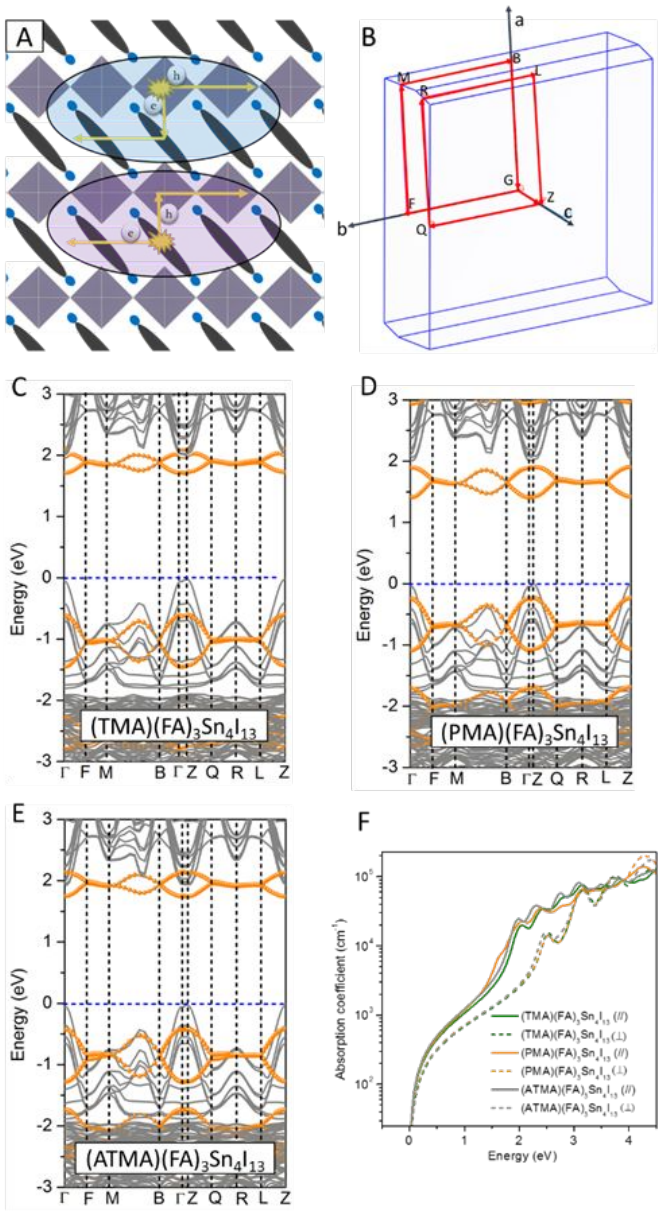

Figure 3. (A) Mechanism of charge transfer in 2D OIHPs with the type-II band alignment. (B) The *K* path in the reciprocal space. (C-E) Computed band structures (based on the PBE0 functional) of $(TMA)(FA)_3Sn_4I_{13}$ (C), $(PMA)(FA)_3Sn_4I_{13}$ (D) and $(ATMA)(FA)_3Sn_4I_{13}$ (E). (F) Computed optical absorption spectra (based on the PBE0 functional) of $(TMA)(FA)_3Sn_4I_{13}$, $(PMA)(FA)_3Sn_4I_{13}$ and $(ATMA)(FA)_3Sn_4I_{13}$ (//: parallel to xy; ⊥: perpendicular to xy plane).

The electronic properties of the three compounds, which possess both features of organic semiconductor and inorganic tin halide perovskites, can be viewed as a combination of those of 2D tin perovskite and oligoacene. In addition, we have computed optoelectronic properties of 2D tin perovskite ($(MA)_2(FA)_3Sn_4I_{13}$), 2D tetracenes, 2D pentacenes, and 2D anthra[2,3-*b*:7,8-*b*']dithiophene (see Electronic Supplemental Information (ESI) Fig. S12 for more details). ESI Figs. S13-S16 show computed optoelectronic properties of the four 2D materials, including the band structures, PDOS, and optical absorption spectra (//: parallel to xy ; ⊥ : perpendicular to xy plan). All the four 2D materials exhibit direct bandgap at the Γ point. The band structures and PDOS of $(MA)_2(FA)_3Sn_4I_{13}$ exhibit similar characters as 3D tin perovskites, except the wider bandgap. The light absorption in "//" direction is slightly stronger than that in the " ⊥ " direction in the visible range. Other three "organic" 2D materials exhibit similar band structures and PDOS due to their similar π-conjugation structure and arrangement of molecules. The three "organic" 2D materials also exhibit strong light absorption in the visible region; while the "//" light absorption is stronger than the " ⊥ " one in the visible region due to the orientation of molecules.

In view of different optical absorption region for the organic and inorganic component, suitable mix of the inorganic and organic 2D materials can enable absorption of solar light in wider region (e.g., from ultraviolet or infrared) to enhance the performance of PV. Akin to the principle underlying the tandem solar cells, when crystal orientations of organic and inorganic components in 2D OIHPs are perpendicular to the substrate, the PV device can be viewed as parallel stacking of a series of solar cells. Because of strong light absorption in the visible region for the "inorganic" and "organic" components, $(TMA)(FA)_3Sn_4I_{13}$, $(PMA)(FA)_3Sn_4I_{13}$ and $(ATMA)(FA)_3Sn_4I_{13}$ exhibit stronger absorption in the visible region (see Fig. 3F), which may be beneficial to the performance of PV. Analogous to the corresponding 2D material, the "//" light absorption is also stronger than " ⊥ " in visible range.

For OIHPs containing tin element, the spin-orbit coupling (SOC) can moderately reduce the bandgap. Fig. S17 shows computed DOS of $(TMA)(FA)_3Sn_4I_{13}$, $(PMA)(FA)_3Sn_4I_{13}$ and $(ATMA)(FA)_3Sn_4I_{13}$, based on the PBE0 functional with considering SOC effect. Clearly, the states of "organic" component are little effected by the SOC. In stark contrast, the CBM of "inorganic" component shifts to a lower energy level by about 0.25 eV, compared to that without considering SOC. This is because the CBM is mostly contributed by Sn *p* orbitals. Still, the three compounds considered maintain the type-IIb band alignment. Moreover, we perform *ab* initio molecular dynamic (AIMD) simulations to examine thermal stabilities of the three compounds at 300 K (see Fig. S18). It can be seen that these 2D perovskite frameworks are well sustained during the AIMD simulation, suggesting that these compounds are likely to be thermal stable at room temperature.

Carrier mobility is another important property for PV performance assessment. The "inorganic" component of 2D tin OHIPs exhibits relatively high carrier mobility. For example, PEA_2SnI_4 (PEA = $C_6H_5C_2H_4NH_3^+$) exhibits a hole mobility as high as 26 $cm^2V^{-1}S^{-1}$ and an electron mobility of 4.6 $cm^2V^{-1}S^{-1}$.[47, 48] Due to the band offset between the conduction and valence band of "inorganic" and "organic" components, electrons and holes are promoted to transfer between "inorganic" and "organic" components, respectively. For newly designed compounds, it would be desirable that the "organic" component also possesses relatively high carrier mobility. Note that due to the symmetry of 2D OIHPs and the π-DAMs, there is only a

weak dipole interaction between the ammoniums and iodine ions. The main π-conjugation structures of π-DAMs are not strongly affected by the "inorganic" component, retaining similar optoelectronic properties of π-DAMs as the corresponding organic molecules. As such, we can use the Marcus theory to assess charge carrier mobility of the three π-DAMs. The computed reorganization energies for electron and hole transfer are listed in Table S1. For π-conjugation cations which are electron-rich systems, negative polaronic state exhibits stronger deformation than positive polaronic state, resulting in higher reorganization energy. The electronic couplings based on the two different charge hopping channels (see Fig. 4) are listed in Tables S2-S4. One can see that the electronic couplings for the electron transfer are slightly weaker than those for the hole transfer. The computed electron mobility is 0.51, 2.06 and 0.23 $cm^2V^{-1}S^{-1}$ for TMA, PMA and ATMA, respectively, while the computed hole mobility is 5.24, 6.25 and 5.42 $cm^2V^{-1}S^{-1}$ for TMA, PMA and ATMA, respectively. The electron mobility is slightly lower than the hole mobility, consistent with previous report.[46] The charge carrier mobilities are also much higher than those of other organic cations used in 2D OIHPs due to strong overlap between the π-π stacking of molecular structures. The carrier mobility of "organic" component is comparable to that of amorphous silicon (0.5−1.0 $cm^2V^{-1}S^{-1}$), indicating that the three compounds would likely exhibit high carrier mobility. This accounts for two parallel high-speed channels for hole and electron transfer, respectively. In addition, we have computed carrier mobility of the corresponding 2D organic materials (tetracenes, pentacenes and anthra[2,3-*b*:7,8-*b*']dithiophene). Due to the smaller reorganization energies of organic molecules (with respect to inorganic counterparts), all three 2D organic materials are predicted to exhibit higher carrier mobility than those of π-DAMs (see Tables S5-S8). Although the carrier mobility of π-DAMs exhibits a decline, the π-DAMs still retain the main feature of carrier mobility. So it is sensible to pre-estimate the properties of charge transfer of "organic" component for 2D OIHPs via computing the carrier mobility of corresponding organic molecules.

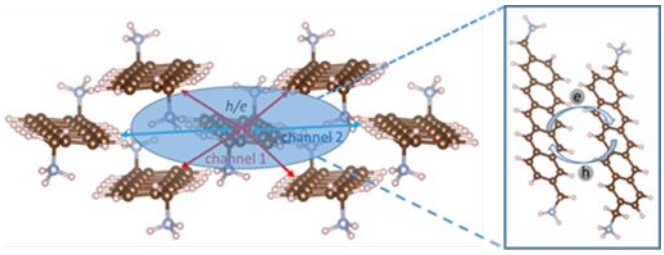

Figure 4. Schematic of charge carrier hopping channels for calculating the charge carrier mobility of TMA, PMA and ATMA. The π–π stacking of π-DAMs could facilitate the charge transfer.

Lastly, we note that 2D perovskites containing large aromatic organic components (oligothiophenes and divalent benzodiimidazolium) have already been synthesized in previous experiments.[42, 43, 49] Very recently, a 2D DJ perovskite solar cell based on benzene dimethanammonium cation has achieved PCE of 15.6%.[50] We expect that more 2D DJ perovskites based on larger aromatic (like AMA, TMA and PMA etc.) diammonium will be synthesized in near future. To fabricate the PV device based on the 2D DJ perovskites with larger aromatic diammonium, it is important to synthesize the film of 2D DJ OIHPs. In a previous work,[32] 2D OIHPs thin films were fabricated by using a hot-casting technique. Through this synthesis route, the inorganic and organic sheets' orientations in 2D OIHPs are both perpendicular to the substrate in the thin films (see Fig. S19). The band offset between the conduction band and valence band can lead to separation of electron and hole between the organic and inorganic sheets, and to the suppression of electron/hole recombination, thereby enhancing the performance of the PV device.

Conclusions

In conclusion, we have investigated a series of 2D lead-free OIHPs, (diammonium)$(FA)_{n-1}Sn_nX_{3n+1}$ (n = 1 - 4), as potentially high-performance light absorbers for PV applications. By carefully choosing proper organic functional cations, the 2D compounds can possess different band alignment (among type-Ia, -Ib, -IIa and -IIb) by design. The optoelectronic properties are also tunable, by using different functionalization approaches, such as changing the halogen atom, π-conjugation diammounium, and layers of "inorganic" component. More specifically, we identify three compounds, $(TMA)(FA)_3Sn_4I_{13}$, $(PMA)(FA)_3Sn_4I_{13}$ and $(ATMA)(FA)_3Sn_4I_{13}$, to possess type-II band alignment and high carrier mobility in their "organic and inorganic" component. Considering that both visible-light absorption and carrier mobilities are two key properties of solar cell absorbers, we predict that the newly predicted three compounds are promising candidates to yield reasonably high performance while can also address both stability and lead-toxicity issues elucidated in the introduction for future PV application.

Electronic Supplementary Information

ESI is available from the Wiley Online Library or from the author. Computational methods. Additional calculations and analysis data in Figures S1−S19 and Tables S1−S8.

Acknowledgements

X.C.Z. was supported by the National Science Foundation (NSF) through the Nebraska Materials Research Science and Engineering Center (MRSEC) (grant No. DMR-1420645), an NSF EPSCoR Track 2 grant (OIA-1538893), and by the University of Nebraska Holland Computing Center.

Notes and references

1 https://www.nrel.gov/pv/assets/pdfs/pv-efficiency-chart.20181221.pdf.
2 F. De Angelis, *ACS Energy Lett.*, 2018, **3**, 890-891.
3 J.-P. Correa-Baena, M. Saliba, T. Buonassisi, M. Grätzel, A. Abate, W. Tress and A. Hagfeldt, *Science*, 2017, **358**, 739-744
4 Q. Han, Y.-T. Hsieh, L. Meng, J.-L. Wu, P. Sun, E.-P. Yao, S.-Y.

Chang, S.-H. Bae, T. Kato and V. Bermudez, *Science*, 2018, **361**, 904-908
5 J. Huang, Y. Yuan, Y. Shao and Y. Yan, *Nat. Rev. Mater.*, 2017, **2**, 17042.
6 M. M. Lee, J. Teuscher, T. Miyasaka, T. N. Murakami and H. J. Snaith, *Science*, 2012, **338**, 643-647
7 A. Mei, X. Li, L. Liu, Z. Ku, T. Liu, Y. Rong, M. Xu, M. Hu, J. Chen and Y. Yang, *Science*, 2014, **345**, 295-298
8 N.-G. Park, M. Grätzel, T. Miyasaka, K. Zhu and K. Emery, *Nat. Energy*, 2016, **1**, 16152.
9 A. Walsh, *J. Phys. Chem. C*, 2015, **119**, 5755-5760
10 W. Wei, Y. Zhang, Q. Xu, H. Wei, Y. Fang, Q. Wang, Y. Deng, T. Li, A. Gruverman and L. Cao, *Nat. Photonics*, 2017, **11**, 315
11 O. Yaffe, Y. Guo, L. Z. Tan, D. A. Egger, T. Hull, C. C. Stoumpos, F. Zheng, T. F. Heinz, L. Kronik and M. G. Kanatzidis, *Phys. Rev. Lett.*, 2017, **118**, 136001.
12 M.-G. Ju, M. Chen, Y. Zhou, H. F. Garces, J. Dai, L. Ma, N. P. Padture and X. C. Zeng, *Joule*, 2018, **2**, 1231.
13 M. Chen, M.-G. Ju, A. D. Carl, Y. Zong, R. L. Grimm, J. Gu, X. C. Zeng, Y. Zhou and N. P. Padture, *Joule*, 2018, **2**, 558-570.
14 D. Meggiolaro, S. G. Motti, E. Mosconi, A. J. Barker, J. Ball, C. A. R. Perini, F. Deschler, A. Petrozza and F. De Angelis, *Energy Environ. Sci.*, 2018, **11**, 702-713.
15 L. Ma, M.-G. Ju, J. Dai and X. C. Zeng, *Nanoscale*, 2018, **10**, 11314-11319.
16 P. Ramasamy, D.-H. Lim, B. Kim, S.-H. Lee, M.-S. Lee and J.-S. Lee, *Chem. Commun.*, 2016, **52**, 2067-2070.
17 C. C. Stoumpos, L. Frazer, D. J. Clark, Y. S. Kim, S. H. Rhim, A. J. Freeman, J. B. Ketterson, J. I. Jang and M. G. Kanatzidis, *J. Am. Chem. Soc*, 2015, **137**, 6804-6819.
18 E. Mosconi, A. Amat, M. K. Nazeeruddin, M. Grätzel and F. De Angelis, *J. Phys. Chem. C*, 2013, **117**, 13902-13913.
19 D. Meggiolaro and F. De Angelis, *ACS Energy Lett.*, 2018, **3**, 2206-2222
20 M. G. Ju, J. Dai, L. Ma and X. C. Zeng, *J. Am. Chem. Soc.*, 2017, **139**, 8038-8043.
21 F. Zhang, D. H. Kim, H. Lu, J.-S. Park, B. Larson, J. Hu, L. Gao, C. Xiao, O. Reid and X. Chen, *J. Am. Chem. Soc.*, 2019, **141**, 5972-5979.
22 D. H. Cao, C. C. Stoumpos, O. K. Farha, J. T. Hupp and M. G. Kanatzidis, *J. Am. Chem. Soc.*, 2015, **137**, 7843-7850
23 Y. Chen, Y. Sun, J. Peng, J. Tang, K. Zheng and Z. Liang, *Adv. Mater.*, 2018, **30**, 1703487.
24 L. Mao, K. C. Stoumpos and M. G. Kanatzidis, *J. Am. Chem. Soc.*, 2018, DOI: 10.1021/jacs.1028b10851.
25 A. H. Proppe, R. Quintero-Bermudez, H. Tan, O. Voznyy, S. O. Kelley and E. H. Sargent, *J. Am. Chem. Soc.*, 2018, **140**, 2890-2896
26 L. N. Quan, M. Yuan, R. Comin, O. Voznyy, E. M. Beauregard, S. Hoogland, A. Buin, A. R. Kirmani, K. Zhao and A. Amassian, *J. Am. Chem. Soc.*, 2016, **138**, 2649-2655
27 I. C. Smith, E. T. Hoke, D. Solis-Ibarra, M. D. McGehee and H. I. Karunadasa, *Angew. Chem.*, 2014, **126**, 11414-11417
28 N. Zhou, Y. Shen, L. Li, S. Tan, N. Liu, G. Zheng, Q. Chen and H. Zhou, *J. Am. Chem. Soc.*, 2017, **140**, 459-465
29 M.-G. Ju, J. Dai, L. Ma, Y. Zhou and X. C. Zeng, *J. Am. Chem. Soc.*, 2018, **140**, 10456-10463.
30 L. Ma, J. Dai and X. C. Zeng, *Adv. Energy Mater.*, 2017, **7**, 1601731.
31 L. Pedesseau, D. Sapori, B. Traore, R. Robles, H.-H. Fang, M. A. Loi, H. Tsai, W. Nie, J.-C. Blancon and A. Neukirch, *ACS nano*, 2016, **10**, 9776-9786.
32 H. Tsai, W. Nie, J.-C. Blancon, C. C. Stoumpos, R. Asadpour, B. Harutyunyan, A. J. Neukirch, R. Verduzco, J. J. Crochet and S. Tretiak, *Nature*, 2016, **536**, 312.
33 H. Tsai, R. Asadpour, J.-C. Blancon, C. C. Stoumpos, J. Even, P. M. Ajayan, M. G. Kanatzidis, M. A. Alam, A. D. Mohite and W. Nie, *Nat. Commun.*, 2018, **9**, 2130
34 X. Zhang, X. Ren, B. Liu, R. Munir, X. Zhu, D. Yang, J. Li, Y. Liu, D.-M. Smilgies and R. Li, *Energy Environ. Sci.*, 2017, **10**, 2095-2102.
35 L. Mao, W. Ke, L. Pedesseau, Y. Wu, C. Katan, J. Even, M. R. Wasielewski, C. C. Stoumpos and M. G. Kanatzidis, *J. Am. Chem. Soc.*, 2018, **140**, 3775-3783
36 M. Chen, M.-G. Ju, M. Hu, Z. Dai, Y. Hu, Y. Rong, H. Han, X. C. Zeng, Y. Zhou and N. P. Padture, *ACS Energy Lett.*, 2019, **4**, 276-277.
37 D. B. Straus and C. R. Kagan, *J. Phys. Chem. Lett.*, 2018, **9**, 1434-1447
38 D. B. Mitzi, K. Chondroudis and C. R. Kagan, *IBM J. Res. Dev.*, 2001, **45**, 29-45
39 L. Mao, H. Tsai, W. Nie, L. Ma, J. Im, C. C. Stoumpos, C. D. Malliakas, F. Hao, M. R. Wasielewski and A. D. Mohite, *Chem. Mater.*, 2016, **28**, 7781-7792
40 J. Gebhardt, Y. Kim and A. M. Rappe, *J. Phys. Chem. C*, 2017, **121**, 6569-6574
41 B. Saparov and D. B. Mitzi, *Chem. Rev.*, 2016, **116**, 4558-4596
42 D. B. Mitzi, K. Chondroudis and C. R. Kagan, *Inorg. Chem.*, 1999, **38**, 6246-6256
43 M. Braun, W. Tuffentsammer, H. Wachtel and H. C. Wolf, *Chem. Phys. Lett.*, 1999, **303**, 157-164.
44 C. Liu, W. Huhn, K.-Z. Du, A. Vazquez-Mayagoitia, D. Dirkes, W. You, Y. Kanai, D. B. Mitzi and V. Blum, *Phys. Rev. Lett.*, 2018, **121**, 146401.
45 T. P. Nguyen, J. H. Shim and J. Y. Lee, *J. Phys. Chem. C*, 2015, **119**, 11301-11310.
46 V. Coropceanu, J. Cornil, D. A. da Silva Filho, Y. Olivier, R. Silbey and J.-L. Brédas, *Chem. Rev.*, 2007, **107**, 926-952 %@ 0009-2665.
47 T. Matsushima, S. Hwang, S. Terakawa, T. Fujihara, A. S. D. Sandanayaka, C. Qin and C. Adachi, *Appl. Phys. Express*, 2017, **10**, 024103
48 T. Matsushima, S. Hwang, A. S. D. Sandanayaka, C. Qin, S. Terakawa, T. Fujihara, M. Yahiro and C. Adachi, *Adv. Mater.*, 2016, **28**, 10275-10281
49 I. Zimmermann, S. Aghazada and M. K. Nazeeruddin, *Angew. Chem. Int. Ed.*, 2019, **58**, 1072-1076.
50 B. E. Cohen, Y. Li, Q. Meng and L. Etgar, *Nano Lett.*, 2019, DOI: 10.1021/acs.nanolett.1029b00387.

Table of contents entry